Check for updates

AGU ADVANCING EARTH AND SPACE SCIENCE

Geophysical Research Letters

RESEARCH LETTER
10.1029/2020GL090425

Key Points:

- Monsoon low-pressure systems that achieve greater intensity are more likely to undergo genesis in active phases of intraseasonal variability
- Genesis of these developing systems is accompanied by large-scale, zonally elongated anomalies of moist static energy and vorticity
- The northward propagating intraseasonal oscillation may foster monsoon depression intensification by preconditioning the atmosphere

Supporting Information:

- Supporting Information S1

Correspondence to:
N. Karmakar,
nirupam.ju@gmail.com;
nkarmakar@fsu.edu

Citation:
Karmakar, N., Boos, W. R., & Misra, V. (2021). Influence of intraseasonal variability on the development of monsoon depressions. *Geophysical Research Letters*, *48*, e2020GL090425. https://doi.org/10.1029/2020GL090425

Received 18 AUG 2020
Accepted 11 DEC 2020

© 2020. American Geophysical Union. All Rights Reserved.

Influence of Intraseasonal Variability on the Development of Monsoon Depressions

Nirupam Karmakar[1,2,3], William R. Boos[4,5], and Vasubandhu Misra[1,6,7]

[1]Earth, Ocean and Atmospheric Science Department, Florida State University, Tallahassee, FL, USA, [2]Now at Indian Institute of Tropical Meteorology, Pune, Maharashtra, India, [3]Now at National Centre for Medium Range Weather Forecasting, Ministry of Earth Sciences, Noida, Uttar Pradesh, India, [4]Department of Earth and Planetary Science, University of California, Berkeley, CA, USA, [5]Climate and Ecosystem Sciences Division, Lawrence Berkeley National Laboratory, Berkeley, CA, USA, [6]Center for Ocean-Atmospheric Prediction Studies, Florida State University, Tallahassee, FL, USA, [7]Florida Climate Institute, Florida State University, Tallahassee, FL, USA

Abstract Previous studies showed that the activity of monsoon low-pressure systems (LPS), which produce a large fraction of the South Asian monsoon's total rainfall, is modulated by intraseasonal variability. Using satellite-derived products and atmospheric reanalyzes, this study examines how the boreal summer intraseasonal oscillation (ISO) separately modulates the occurrence of weaker LPS (lows) and stronger LPS (depressions). It is found that the genesis of lows is insensitive to ISO phase, while depressions exhibit a strong preference for genesis during the phase that is convectively active over the northern Indian Ocean. Essentially, development of LPS into depressions depends upon the timing of genesis of the initial disturbance. Evidence is presented supporting the hypothesis that the development of lows into depressions is fostered by large-scale atmospheric conditions governed by the ISO. Results also suggest that while lows have no preference for forming over ocean compared to land, depressions mostly form over ocean.

Plain Language Summary Low-pressure systems (LPS) with lifetimes of about 5 days are a major component of the South Asian summer monsoon, contributing nearly half of the total seasonal rainfall in large parts of South Asia. Intraseasonal variability manifesting as northward propagation of rain bands from the equator to the foothills of the Himalayas on 20–60 days time scales has been shown to modulate the occurrence of LPS. Here, we investigate how intraseasonal variability separately modulates the occurrence of weaker LPS (lows) and stronger LPS (depressions). We find that genesis of lows is insensitive to the phase of intraseasonal variability, while depressions mostly form over the northern Bay of Bengal when intraseasonal variability produces positive rainfall anomalies within that region. Furthermore, LPS that intensify into depressions tend to form preferentially over oceans. We present evidence suggesting that intraseasonal variability preconditions the large-scale atmosphere, enhancing the environmental moisture and vorticity during the genesis of LPS that develop into depressions.

1. Introduction

Intraseasonal oscillations (ISOs) in the Indian summer monsoon represent dominant modes of variability of that circulation (Sikka & Gadgil, 1980; Yasunari, 1979). One of the most prominent manifestations of these ISOs is characterized by northward propagation of rain bands from the equatorial Indian Ocean to the foothills of the Himalayas with a periodicity of 20–60 days (Ajaya Mohan & Goswami, 2003; Karmakar et al., 2017a; Krishnamurthy & Shukla, 2007). This ISO is often associated with an eastward-propagating planetary-scale circulation traveling at a speed of almost 8° longitude/day (Krishnamurti et al., 1985) that is commonly referred to as the Madden–Julian oscillation (Karmakar & Krishnamurti, 2019; Madden & Julian, 1972; Pai et al., 2011; Singh et al., 1992). Active-break cycles of rainfall over India during the monsoon season are often associated with the passage of this ISO (Karmakar et al., 2017a; Rajeevan et al., 2010).

Here, we examine the association of this ISO with synoptic-scale precipitating vortices, also known as low-pressure systems (LPS). In South Asia, weaker LPS are typically called monsoon lows and stronger ones are called monsoon depressions. These lows and depressions together account for around half of the total rainfall over India (Hunt & Fletcher, 2019; Yoon & Chen, 2005), shaping the nature of seasonal

rainfall there. Intraseasonal modes of variability are reported to modulate the genesis of LPS in South Asia (Goswami et al., 2003; Krishnamurthy & Ajayamohan, 2010; Hatsuzuka & Fujinami, 2017). Although the amplitude of intraseasonal variability does not seem to modulate the spatial climatology of monsoon disturbances in the global tropics, occurrences of these disturbances are related to the phase of the ISO (Haertel & Boos, 2017). Goswami et al. (2003) suggested that the frequency of occurrence of LPS over the Indian region is nearly 3.5 times higher in active phases of the ISO compared to break phases. However, these studies did not look into lows and depressions separately. Also, Goswami et al. (2003) defined the ISO as the 10–90 days filtered relative vorticity at 850 hPa averaged over the "core monsoon" region. Thus, the ISO index used in their study could have effects from two types of ISO: a higher-frequency westward-propagating 10–20 days mode (Karmakar et al., 2017a; Krishnamurti & Bhalme, 1976) and the lower-frequency northward-propagating 20–60 days mode. There is not a large-scale separation between the higher-frequency mode and synoptic-scale LPS; indeed, Krishnamurthy and Ajayamohan (2010) noted that days with LPS over India have a rainfall pattern resembling the active period of the monsoon, while days without LPS have rainfall similar to that of the break monsoon.

We aim to understand how the genesis and development of LPS depends upon the phases of the northward-propagating 20–60 days ISO mode, which has a clearer scale separation with synoptic-scale LPS. We focus on the separate modulation of lows and depressions by this ISO, unlike previous work that studied LPS activity in aggregate. We also examine what large-scale atmospheric features associated with the ISO might contribute to LPS genesis and development, building on recent studies that argue that monsoon depression amplification can be accomplished through barotropic growth in the meridionally sheared low-level monsoon westerlies (Diaz & Boos, 2019a, 2019b) and through coupling with the background moist static energy (MSE) field (Adames & Ming, 2018). Our analyses may help in understanding differences between developing and nondeveloping LPS.

2. Data Set and Methodology

We use the monsoon LPS track data set developed by Hurley and Boos (2015), which was created using an objective algorithm (Hodges, 1994) to identify 850 hPa relative vorticity maxima in the European Center for Medium-Range Weather Forecasts (ECMWF) ReAnalysis (ERA)-Interim (Dee et al., 2011) for 1979–2012. Vorticity maxima were required to be localized in both latitude and longitude, and to have a minimum lifetime of 2 days, similar to prior studies using the same algorithm to track a variety of tropical disturbances (Hodges et al., 2003; Thorncroft & Hodges, 2001); Hurley and Boos (2015) furthermore required disturbances to have a minimum sea level pressure anomaly with amplitude ≥2 hPa, relative to a 21 days running mean and within 500 km of the 850 hPa vortex center. The resulting LPS were classified as "lows," "depressions," and "deep depressions" based on their sea level pressure anomaly and maximum surface wind speed (Hurley & Boos, 2015). We focus on LPS developing in boreal summer (May–October) over the South Asian region. We use atmospheric fields from ERA-Interim (Dee et al., 2011) (https://apps.ecmwf.int/datasets/), converting six-hourly data to daily means. We also use Tropical Rainfall Measuring Mission (TRMM) 3B42 (V7) daily rainfall data (Huffman et al., 2007) (https://pmm.nasa.gov/data-access/), available from 1998 onwards, to diagnose ISO modes in rainfall. Therefore, our period of analysis is 1998–2012, the common period of data availability for all data sets. However, we also test the robustness of our results using a recently developed LPS data set that was compiled with an optimized algorithm that tracks 850 hPa stream function anomalies in the ERA5 reanalysis (Vishnu et al., 2020), together with the TRMM Multisatellite Precipitation Analysis daily accumulated rainfall product (https://disc.gsfc.nasa.gov/datasets/TRMM_3B42_Daily_7/summary;%201998–2019) and interpolated outgoing longwave radiation (OLR; 1979–2018) (Liebmann & Smith, 1996); provided by the NOAA/OAR/ESRL PSL (Boulder, Colorado, USA).

Daily climatologies are calculated as the mean of each calendar day over the entire time period used in the analysis. Daily anomalies are calculated by removing this daily climatology (smoothed using the first two seasonal harmonics) from daily data. Bootstrapping is used for assessing statistical significance of results.

2.1. Extraction of ISO Modes

Multichannel singular spectrum analysis (MSSA) is used to extract ISOs in rainfall over the South Asian region (4°N–37°N, 50°E–101°E) (Ghil et al., 2002; Plaut & Vautard, 1994). This data-adaptive filtering technique is useful in extracting oscillatory signals from short and noisy time series and has been used in many studies recently in the context of the Indian monsoon (Karmakar et al., 2017a; Krishnamurthy & Shukla, 2007; Moron et al., 2012). Prefiltering is applied to rainfall anomalies at each grid point with a 5 days moving mean to remove high-frequency fluctuations. Each year's May–October data are then fed into the MSSA algorithm, which finds oscillatory modes in the data. Lagged copies (using a window length of 60 days) of the data are augmented to construct a lag-covariance matrix, which is diagonalized to obtain space–time empirical orthogonal functions and principal components. Then, using the significant modes (a test is performed with 1,000 red-noise surrogates to determine the significant modes; Allen & Robertson, 1996) that represent oscillation within 20–60-day periods, we can reconstruct the oscillatory part of the ISO. Once the ISO is extracted, we use a principal component analysis on these data to divide the phase plane associated with the ISO into eight equal intervals. Phase compositing of the ISO is done by averaging the classified days based on their phases (Moron et al., 1998). Further, we consider only those days when the ISO exhibits "strong" amplitude (see Supplementary Information [SI] and Figure S1). Results are qualitatively similar when we do not consider ISO amplitude (Figure S2).

3. Results

Figure 1(a) shows the phase-composite diagram of rainfall in the ISO (with a 20–60-day period) during May–October 1998–2012. The eight panels, which are circular in nature and about 3–5 days apart, exhibit northward propagation of rain bands from the equatorial region to the foothills of the Himalayas. Phases 1–3 are associated with negative rainfall anomalies over central India, the Arabian Sea, and Bay of Bengal. This negative anomaly propagates northward and a northwest-southeast tilted large-scale positive anomaly gets established over central India in phases 5–7. We thus define the ISO break period as phases 1–3 and the active period as phases 5–7.

We now examine how the genesis of LPS, and of the individual categories of lows and depressions, is modulated by the ISO. During summer (May–October) from 1998 to 2012, 237 lows, 97 depressions, and 8 deep depressions were observed. We categorize these according to the ISO phase in which they are first detected (day 0 of their track), using only days when the ISO is strong (Figure 1(b)). The lows show no preference in genesis with respect to ISO phase, whereas depressions show a strong preference for forming during the active period (phases 5–7). Figure 1(b) shows that the number of LPS is larger in the active period (96) than the break period (71). The number of lows is nearly the same in active and break periods (56 and 58, respectively), while 40 depressions/deep depressions underwent genesis in active periods and only 13 in breaks. Thus, only 18% of LPS that had genesis during break periods intensified into depressions/deep depressions, compared to 42% of LPS originating in active periods. To be clear, all depressions evolve from lows, and LPS are categorized according to the phase in which the low is first detected, not the phase in which the low intensified to a depression. Deep depressions are rare (only three in number; two in active periods) and so are not considered in the below composite analysis. Of the 38 depressions that formed in the active period, 33 formed over ocean. In contrast, lows in the active period do not show such a preference for forming over the ocean, with 32 of 56 lows in the active period forming over land. Tracks of all of these storms are shown in Figure S3. Most depressions in the active period form over the northern Bay of Bengal and propagate westward to central and northwestern India, which may be relevant because the northern Bay of Bengal is the region where the rate at which energy can be extracted through barotropic conversion for the development of the depressions is maximum (Diaz & Boos, 2019a). There is no detectable association of the duration of LPS with the ISO phase in which they undergo genesis (Figure S4). However, disturbances forming over ocean tend to have longer durations. The ERA5 tracks for the longer period of 1998–2019 show similar results (Figure 1(d)), except with a higher number of depressions in ISO phase 3. One third of the ERA5 depressions that form in phase 3 have genesis points over the southern and far southeastern Bay of Bengal (south of 11°N with one at 100°E, not shown), placing these outside the main genesis region of the northern Bay of Bengal. Altogether, these results suggest that LPS that undergo genesis during the active period of the ISO have a higher chance of intensifying into depressions.

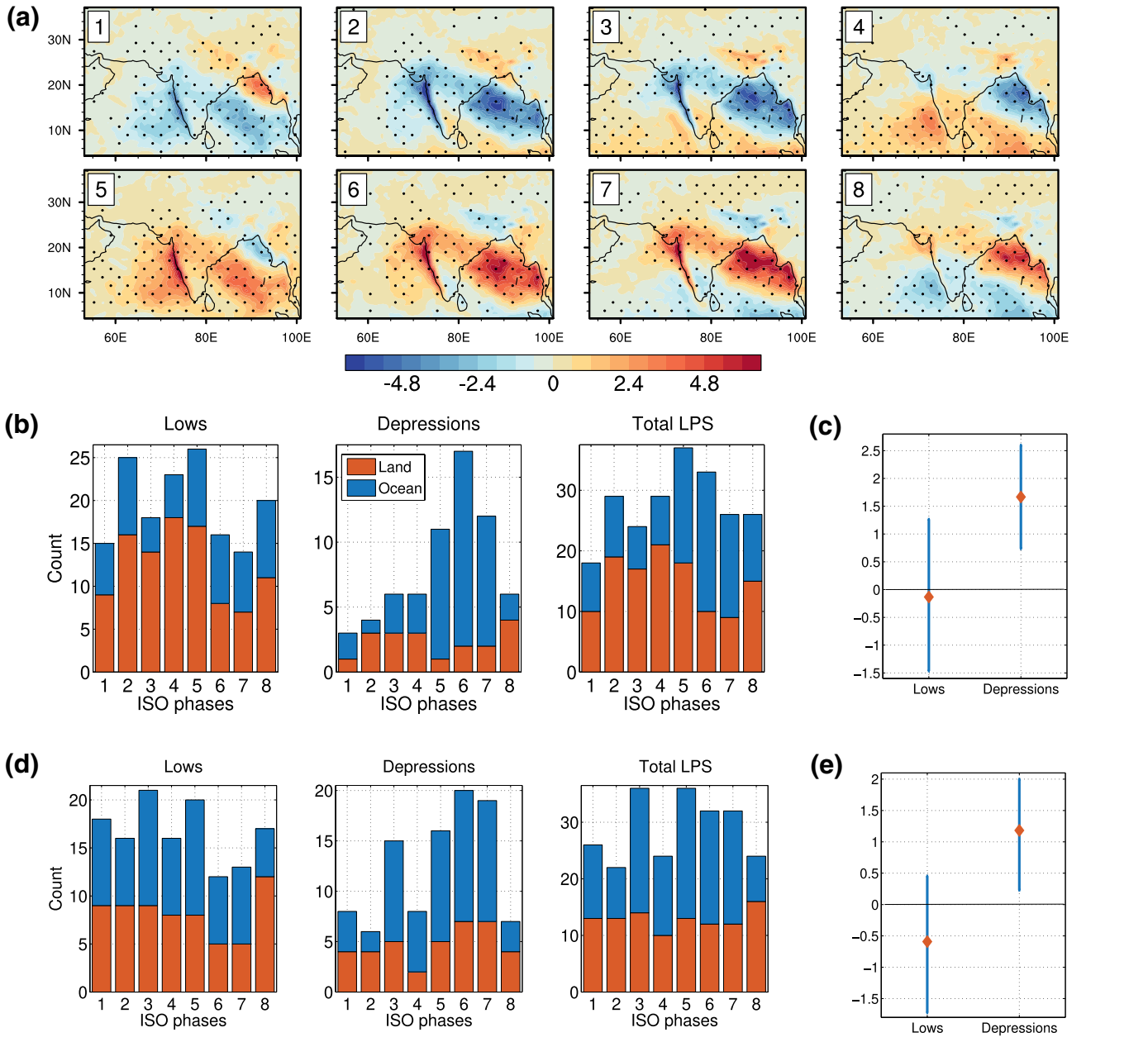

Figure 1. (a) Phase-composite diagram of rainfall ISO (in mm/day) during May–October 1998–2012. Only those days are considered when ISO amplitude is more than one (see SI) or the ISO is "strong." Stippled regions are where values are significant at 5% level. Numbers in the panels indicate the phase numbers. (b) Counts of "lows," "depressions," and "total LPS" with genesis time in different phases of ISO (when ISO is strong) during the same time period from Hurley–Boos data set (1998–2012). Red and blue bars show the values for LPS formed over land and oceans, respectively. (c) Difference between the average number of LPS forming in active and break periods, respectively, during 1998–2012. Blue error bars indicate 95% confidence levels in this difference calculated using 1,000 bootstrap samples. (d, e) Same as (b) and (c), but with ERA5 track data set (1998–2019). ISO, intraseasonal oscillation; LPS, low-pressure systems.

We confirm this general result by averaging the number of depressions forming in active and break periods, finding counts of 2.53 and 0.87 per summer, respectively. In comparison, the genesis rates of lows in active and break periods are 3.73 and 3.87 per summer, respectively. There thus exists a strong preference for LPS that intensify to depressions to have initial genesis in the active period. We better quantify this preference by subtracting genesis counts in the break period from those in the active period, calculating a 95% confidence interval for this difference based on 1,000 bootstrap samples. This confidence interval for depressions does not contain zero for both the ERA-Interim (Figure 1(c)) and ERA5 (Figure 1(e)) track data sets. In contrast,

this difference for lows is close to zero and has a confidence interval that includes zero. There is thus no statistically detectable difference between the genesis rate of lows in active and break phases, but there is such a difference for depressions. The results we present here are consistent with those obtained from a longer time period of 1979–2018, using ERA5 LPS tracks and OLR data to identify ISO phases (Figure S5).

Why do lows not show a preference for genesis in the active period while depressions do? To answer this, we examine whether favorable preconditioning of the atmosphere occurs only during the genesis of LPS that develop into depressions, performing a genesis composite analysis of anomaly fields for lows and depressions during active periods. Of 56 lows that formed during active periods, 35 are eliminated because another LPS already existed on the genesis day; this was done to prevent the genesis composite from containing the signature of a preexisting LPS. Similarly, of 38 depressions that formed during active periods, 13 have a genesis day with no other LPS present in the domain. We also show a composite of all days in active periods; there are 602 active days, of which 117 days are observed without any LPS.

We begin by examining the behavior of MSE (the sum of potential, internal, and latent energies), because cyclonic LPS winds acting on the climatological northward MSE gradient have been argued to cause LPS intensification by advecting high MSE air into the western side of the westward-moving LPS (Adames & Ming, 2018). Vertically integrated (from the surface to the top of the atmosphere) MSE anomalies during the active period of the ISO, without regard for whether an LPS is forming, exhibit maxima over the northern Bay of Bengal and Arabian Sea (Figure 2(a)). These anomalies enhance the climatological northward MSE gradient, but only south of about 15°N and thus not in the region where most LPS form. Vortex-centered composites provide more insight, showing that positive MSE anomalies peak near the LPS center (Figures 2(e) and 2(f)), corresponding to an increase of MSE in the nascent vortex but a reduction in the gradient north of the LPS. The northwest-southeast tilt of the MSE anomaly might have some consistency with advective warming and moistening to the west or might arise from the northwest-southeast tilt of the ISO rain bands; in any case, the MSE anomaly is zonally elongated in the storm-centered composite, being at least 3,000 km in zonal width but half that in meridional width during genesis of depressions in active periods (Figure 2(f)). A positive MSE anomaly over and just west of the vortex center is observed for lows forming in active periods, but this is weaker than that seen in depression genesis and is accompanied by spatially extensive negative MSE anomalies north and south of the genesis point. The composite of days in active periods without any LPS shows negative MSE anomalies over India, the northern Bay of Bengal, and Arabian Sea (Figure 2(b)), indicating behavior distinct from that of active ISO days that accompany LPS genesis. Indeed, the largest MSE anomalies occur during genesis of depressions in the active period (Figure 2(d)), with positive MSE anomalies over the Arabian Sea and Bay of Bengal. Development of positive MSE anomalies over the Indian region starts 2 days before depression genesis (Figure S6). Enhanced vertical shear in zonal winds (the difference between 200 and 850 hPa zonal winds) over the Bay of Bengal and Arabian Sea is also observed (Figure S7). It can be difficult to separate the direct effect of vertical shear on LPS development from the effect of the anomalous meridional MSE gradient, because the shear is in thermal wind balance with the temperature gradient and thus (if relative humidity is roughly constant) is tightly coupled with the meridional MSE gradient.

In contrast to the strong and coherent positive MSE anomalies seen during active periods and during depression genesis in those periods, MSE anomalies are negative or of disparate sign over most of India, Bangladesh, and the Bay of Bengal during the genesis of lows in ISO active periods (Figure 2(c)). MSE anomalies exhibit no coherent large-scale signal near the storm center during break periods (not shown). In fact, MSE anomalies are negative over almost the entire Indian region during break periods (Figure 2(g)). Thus, negative MSE anomalies induced by the ISO might inhibit intensification of lows into depressions during break periods, positive MSE anomalies in active periods foster intensification.

We next inspect composites of vorticity, argued to be relevant for LPS intensification through the mechanism of barotropic instability (Diaz & Boos, 2019a; Lindzen et al., 1983); here, we show only storm-centered genesis composites. A zonally elongated positive anomaly in low-level relative vorticity accompanies depression genesis in the active ISO period (Figure 3(b)). This vorticity strip is spread across nearly 4,000 km in the east-west direction and is possibly linked with the enhanced monsoon trough associated with the ISO over the northern Bay of Bengal and central India region (Figure 1(a)), as well as with the northwest-southeast tilted large-scale structure of cyclonic ISO winds known to extend from the Arabian Sea to

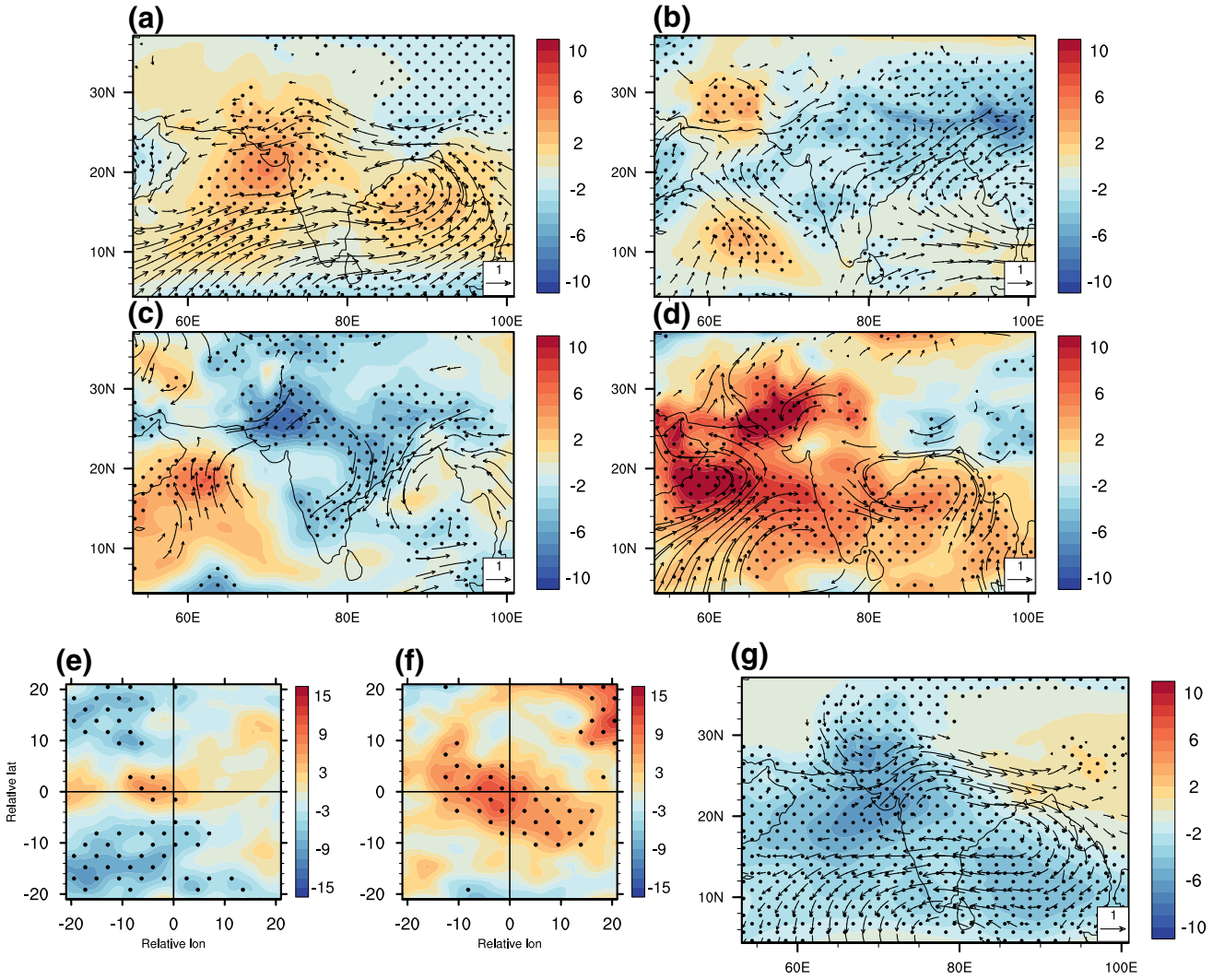

Figure 2. Vertically integrated MSE (10^6J m^{-2}) and winds (m/s) at 850 hPa anomalies during (a) active period of ISO (602 days), (b) active period of ISO but no LPS observed within the region (117 days), (c) genesis day for lows in active periods (21 days), and (d) genesis day for depressions in active periods (13 days). Vortex-centric latitude–longitude diagram of MSE anomalies during genesis day for the (e) lows in active periods and (f) depressions in active periods. (g) Same as (a), but for break periods (597 days). Stippling indicate values are significant at 5% level. Only significant values of wind anomalies in (a)–(d) (at 5% level) are shown. MSE, moist static energy; ISO, intraseasonal oscillation; LPS, low-pressure systems.

the West Pacific (Karmakar & Misra, 2020). This could be also linked to the development of a secondary cyclonic vortex to the west of LPS during large-scale extreme rainfall events (Nikumbh et al., 2020). The vorticity anomaly is weaker and less elongated for lows forming during the active ISO phase (Figure 3(a)). The zonally elongated vortex accompanying depression genesis can be more clearly seen in 850 hPa stream function anomalies (Figure 3(d)), with the statistically significant dynamical structure extending nearly 3,000 km zonally. Stream function and vorticity anomalies are weaker for the genesis of lows, with any zonally elongated structure not passing the threshold for statistical significance, despite the greater number of lows (Figures 3(a) and 3(c)).

Turning back to geographic (as opposed to storm-centered) composites, we see that the large-scale vorticity anomalies that accompany depression genesis manifest as enhanced absolute vorticity over the Bay of Bengal between 15°N and 25°N (Figure 3(e), which shows 850 hPa absolute vorticity averaged 75°E–90°E on the genesis day of lows and depressions). Ditchek et al. (2016) found that enhanced low-level absolute vorticity was correlated, in climatological mean data, with the genesis frequency of the global distribution of monsoon LPS. Mechanistically, amplification of LPS by barotropic instability (Diaz & Boos, 2019a, 2019b)

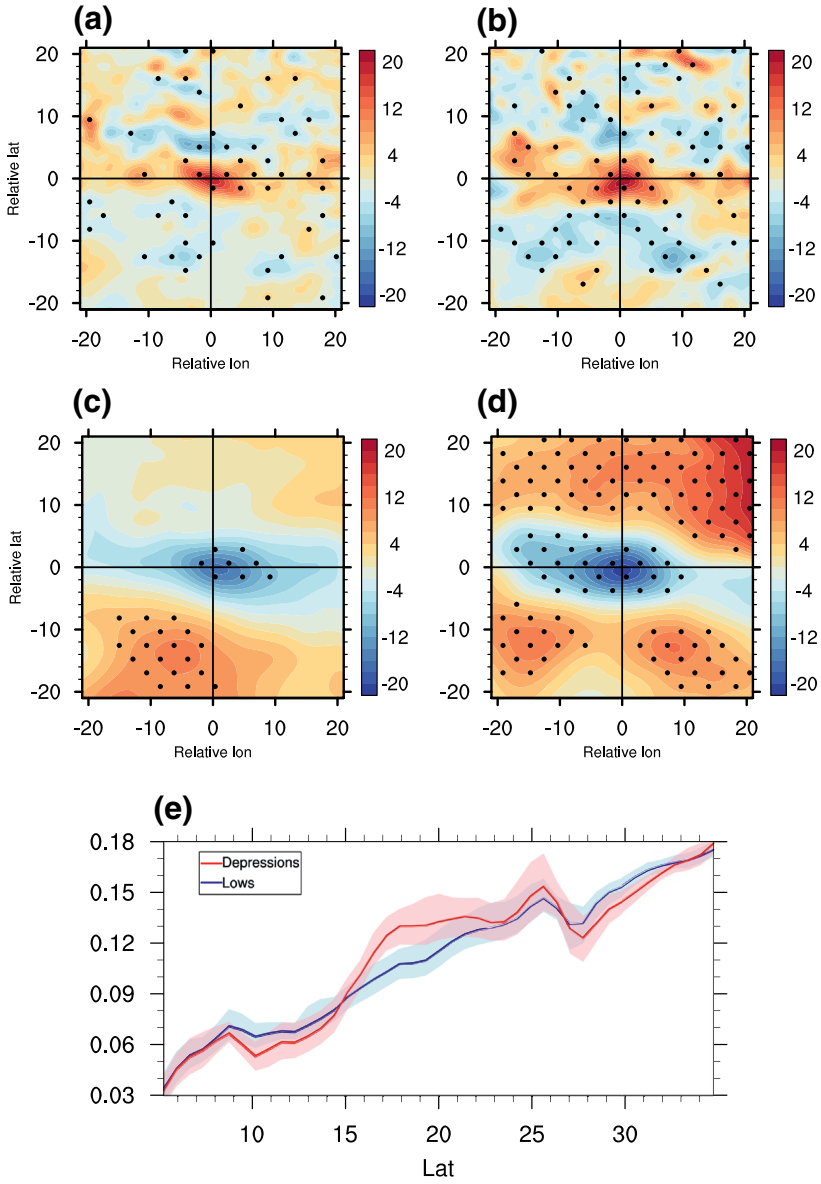

Figure 3. Vortex-centric latitude–longitude diagram of relative vorticity anomalies at 850 hPa level (10^{-6} s^{-1}) during genesis of (a) lows in active periods and (b) depressions in active periods. (c, d) Same as (a) and (b), respectively, but for stream function anomalies at 850 hPa level (10^5 m^2 s^{-1}). Stippling indicate values are significant at 5% level. (e) Latitudinal distribution of vertically integrated (900–700 hPa; normalized by acceleration due to gravity) mean lower level absolute vorticity (kg m^{-2} s^{-1}) averaged between 75°E–90°E during day 0 of lows and depressions in active period. *x* axis denotes latitudes. Shaded areas indicate 95% confidence interval calculated based on 1,000 bootstrap samples.

requires the existence of a local maximum in absolute vorticity, and we generally expect vortex growth rates to increase with environmental low-level absolute vorticity; both the absolute vorticity and the strength of its local maximum are enhanced during the genesis of depressions on active days.

Vertical structures of the atmospheric state are consistent with the hypothesis that the ISO enhances LPS development by fostering low-level barotropic growth, though they also indicate that LPS which develop into depressions are stronger at the time of first detection (i.e., genesis). Vertical columns of positive potential vorticity (PV) anomalies exist at the storm center during genesis of both lows and depressions, but these are more confined to the lower troposphere for LPS that will evolve into depressions (Figures 4(a) and 4(b)). Cyclonic anomalies in low-level zonal wind are significantly stronger, more bottom heavy, and well-defined

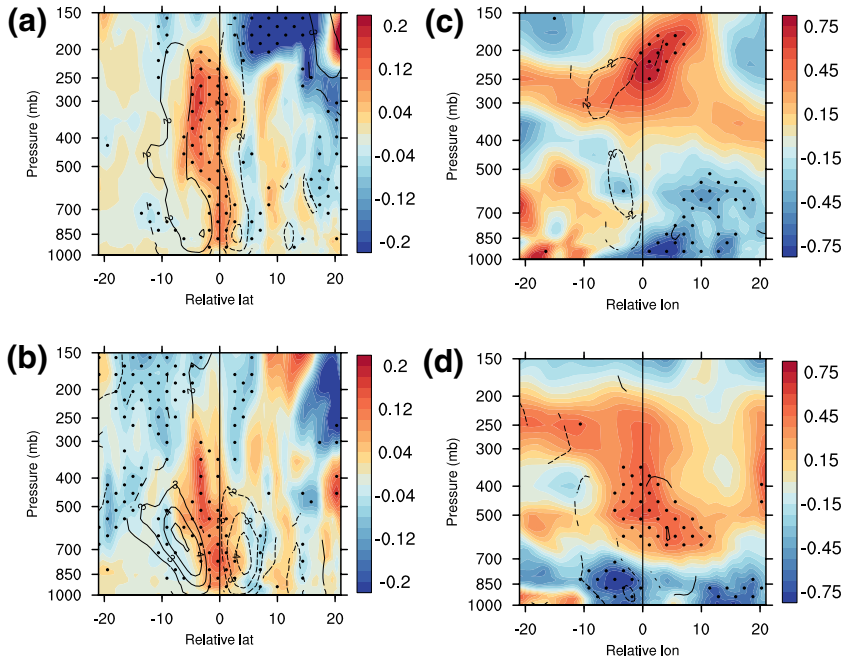

Figure 4. Vortex-centric pressure–latitude section of potential vorticity (PV) anomalies (colors; in $\left(PVU = 10^{-6}\mathrm{Km}^2\mathrm{kg}^{-1}\mathrm{s}^{-1}\right)$) and zonal wind anomalies (contours; in m/s) during genesis of (a) lows in active periods, (b) depressions in active periods. Vortex-centric height–longitude section of potential temperature anomalies (colors; in (K) and meridional wind anomalies (contours; in m/s) during genesis of the (c) lows in active periods and (d) depressions in active periods. Stippling indicate values are significant at 5% level. Only significant values of wind anomalies (at 5% level) are plotted.

during the genesis of depressions in the active ISO period, consistent with a disturbance growing due to a shear instability of the low-level monsoon westerlies (Diaz & Boos, 2019a). Composites of potential temperature anomalies show the warm-over-cold structure expected from thermal wind balance (Figures 4(c) and 4(d)), and the temperature anomalies for depressions resemble those seen in barotropically unstable normal modes of the observed atmospheric state over the northern Bay of Bengal during boreal summer (Diaz & Boos, 2019a, their Figure 4). Although weaker than those in active periods, deep columns of PV with bimodal top-heavy structure in PV and a warm-over-cold anomaly in the storm center are observed for depressions in break periods (Figure S8). Zonal wind anomalies near the storm center are also weaker for break periods than for active periods LPS. Finally, sea surface temperature (SST) variations are known to be strongly associated with the ISO (Karmakar & Krishnamurti, 2019; Sengupta et al., 2001). However, we find that warm SST anomalies of similar magnitude are seen over the Bay of Bengal during genesis of both lows and depressions in active periods (Figure S9).

4. Conclusions

We found that the genesis of lows is largely insensitive to the phase of the northward propagating ISO over South Asia. In contrast, depressions mostly form during the active period, when the ISO enhances moisture, vorticity, and ascent in a zonally elongated band that stretches across central India, the Bay of Bengal, and the Arabian Sea. In other words, LPS that form during the active period of the ISO have a higher probability of intensifying into depressions. Lows do not show any preference for forming over ocean compared to land, but depressions largely form over ocean. Zonally elongated positive anomalies in MSE and low-level vorticity are seen in genesis composites of LPS that originate in ISO active periods and that eventually develop into depressions. This is consistent with the general idea that tropical vortex intensification is favored in moist, vorticity-rich environments (Ditchek et al., 2016) and with the hypothesis that monsoon depression intensification is caused by barotropic growth in the meridionally sheared low-level westerlies (Diaz & Boos, 2019a). We found no strong evidence for an enhanced meridional MSE gradient during the genesis of

depressions, but ISO-induced positive anomalies of MSE may have general connections with theories for moisture-vortex instability (Adames & Ming, 2018). The absence or comparative weakness of such MSE and vorticity features during the genesis of lows in active periods suggests that the intensification of LPS after genesis is sensitive to large-scale preconditioning of the atmosphere near the time of genesis. Active days without LPS activity generally show somewhat break-like anomalies. Thus, the large-scale environment at genesis plays a major role in determining the fate of LPS, with fluctuations in that environment occurring even within ISO active phases. These results are particularly important as the ISO over India has changed recently (Karmakar et al., 2017b). Given that a substantial part of total seasonal rainfall over India is contributed by LPS, seasonal mean rainfall could also undergo a change if the large-scale environment linked with the ISO alters LPS intensification. In this context, our results provide a basis for understanding the development of LPS after genesis.

Data Availability Statement

Track data developed by Hurley and Boos (2015) can be accessed from http://worldmonsoons.org/global-monsoon-disturbance-track-dataset/. Track data developed by Vishnu et al. (2020) can be downloaded from https://zenodo.org/record/3890646.

Acknowledgments
N. Karmakar and V. Misra acknowledge NASA grants NNX17AG72G and NNX16AD83G, NSF award number 1606296, and the Earth System Science Organization, Ministry of Earth Sciences, Government of India (MM/SERP/FSU/2014/SSC-02/002). W.R. Boos acknowledges support by the Earth System Science Organization, Ministry of Earth Sciences, Government of India (IITM/MM-II/Univ_California_USA/INT-3) under the Monsoon Mission and from the U.S. Department of Energy, Office of Science, Office of Biological and Environmental Research, Climate and Environmental Sciences Division, Regional and Global Model Analysis Program, under Award DE-SC0019367.

References

Adames, A. F., & Ming, Y. (2018). Interactions between water vapor and potential vorticity in synoptic-scale monsoonal disturbances: Moisture vortex instability. *Journal of the Atmospheric Sciences*, *75*(6), 2083–2106. https://doi.org/10.1175/JAS-D-17-0310.1

Ajaya Mohan, R., & Goswami, B. N. (2003). Potential predictability of the Asian summer monsoon on monthly and seasonal time scales. *Meteorology and Atmospheric Physics*, *84*(1–2), 83–100. https://doi.org/10.1007/s00703-002-0576-4

Allen, M., & Robertson, A. (1996). Distinguishing modulated oscillations from colored noise in multivariate datasets. *Climate Dynamics*, *12*(11), 775–784. https://doi.org/10.1007/s003820050142

Dee, D., Uppala, S., Simmons, A., Berrisford, P., Poli, P., Kobayashi, S., et al. (2011). The ERA-Interim reanalysis: Configuration and performance of the data assimilation system. *Quarterly Journal of the Royal Meteorological Society*, *137*(656), 553–597. https://doi.org/10.1002/qj.828

Diaz, M., & Boos, W. R. (2019). Barotropic growth of monsoon depressions. *Quarterly Journal of the Royal Meteorological Society*, *145*(719), 824–844.

Diaz, M., & Boos, W. R. (2019). Monsoon depression amplification by moist barotropic instability in a vertically sheared environment. *Quarterly Journal of the Royal Meteorological Society*, *145*(723), 2666–2684. https://doi.org/10.1002/qj.3585

Ditchek, S. D., Boos, W. R., Camargo, S. J., & Tippett, M. K. (2016). A genesis index for monsoon disturbances. *Journal of Climate*, *29*(14), 5189–5203.

Ghil, M., Allen, M., Dettinger, M., Ide, K., Kondrashov, D., Mann, M., et al. (2002). Advanced spectral methods for climatic time series. *Reviews of Geophysics*, *40*(1), 1003. https://doi.org/10.1029/2000RG000092

Goswami, B. N., Ajayamohan, R. S., Xavier, P. K., & Sengupta, D. (2003). Clustering of synoptic activity by Indian summer monsoon intraseasonal oscillations. *Geophysical Research Letters*, *30*(8), 1431. https://doi.org/10.1029/2002GL016734

Haertel, P., & Boos, W. R. (2017). Global association of the Madden–Julian oscillation with monsoon lows and depressions. *Geophysical Research Letters*, *44*, 8065–8074. https://doi.org/10.1002/2017GL073625

Hatsuzuka, D., & Fujinami, H. (2017). Effects of the South Asian Monsoon Intraseasonal Modes on Genesis of Low Pressure Systems over Bangladesh. *Journal of Climate*, *30*(7), 2481–2499. https://doi.org/10.1175/JCLI-D-16-0360.1

Hodges, K. I. (1994). A general method for tracking analysis and its application to meteorological data. *Monthly Weather Review*, *122*(11), 2573–2586. https://doi.org/10.1175/1520-0493(1994)122<2573:AGMFTA>2.0.CO;2

Hodges, K. I., Hoskins, B. J., Boyle, J., & Thorncroft, C. (2003). A comparison of recent reanalysis datasets using objective feature tracking: Storm tracks and tropical easterly waves. *Monthly Weather Review*, *131*(9), 2012–2037.

Huffman, G. J., Bolvin, D. T., Nelkin, E. J., Wolff, D. B., Adler, R. F., Gu, G., et al. (2007). The TRMM multisatellite precipitation analysis (TMPA): Quasi-global, multiyear, combined-sensor precipitation estimates at fine scales. *Journal of Hydrometeorology*, *8*(1), 38–55. https://doi.org/10.1175/JHM560.1

Hunt, K. M., & Fletcher, J. K. (2019). The relationship between Indian monsoon rainfall and low-pressure systems. *Climate Dynamics*, *53*, 1859–1871.

Hurley, J. V., & Boos, W. R. (2015). A global climatology of monsoon low-pressure systems. *Quarterly Journal of the Royal Meteorological Society*, *141*(689), 1049–1064.

Karmakar, N., Chakraborty, A., & Nanjundiah, R. S. (2017a). Space–time evolution of the low- and high-frequency intraseasonal modes of the Indian summer monsoon. *Monthly Weather Review*, *145*(2), 413–435. https://doi.org/10.1175/MWR-D-16-0075.1

Karmakar, N., Chakraborty, A., & Nanjundiah, R. S. (2017b). Increased sporadic extremes decrease the intraseasonal variability in the Indian summer monsoon rainfall. *Scientific Reports*, *7*, 7824. https://doi.org/10.1038/s41598-017-07529-6

Karmakar, N., & Krishnamurti, T. N. (2019). Characteristics of northward propagating intraseasonal oscillation in the Indian summer monsoon. *Climate Dynamics*, *52*, 1903–1916. https://doi.org/10.1007/s00382-018-4268-2

Karmakar, N., & Misra, V. (2020). Differences in northward propagation of convection over the Arabian Sea and Bay of Bengal during boreal summer. *Journal of Geophysical Research: Atmospheres*, *125*, e2019JD031648. https://doi.org/10.1029/2019JD031648

Krishnamurthy, V., & Ajayamohan, R. S. (2010). Composite structure of monsoon low pressure systems and its relation to Indian rainfall. *Journal of Climate*, *23*(16), 4285–4305. https://doi.org/10.1175/2010JCLI2953.1

Krishnamurthy, V., & Shukla, J. (2007). Intraseasonal and seasonally persisting patterns of Indian monsoon rainfall. *Journal of Climate*, *20*(1), 3–20. https://doi.org/10.1175/JCLI3981.1

Krishnamurti, T. N., & Bhalme, H. (1976). Oscillations of a monsoon system. Part I. Observational aspects. *Journal of the Atmospheric Sciences*, *33*(10), 1937–1954. https://doi.org/10.1175/1520-0469(1976)033<1937:OOAMSP>2.0.CO;2

Krishnamurti, T. N., Jayakumar, P., Sheng, J., Surgi, N., & Kumar, A. (1985). Divergent circulations on the 30 to 50 day time scale. *Journal of the Atmospheric Sciences*, *42*(4), 364–375. https://doi.org/10.1175/1520-0469(1985)042<0364:DCOTTD>2.0.CO;2

Liebmann, B., & Smith, A. C. (1996). Description of a complete (interpolated) outgoing longwave radiation dataset. *Bulletin of the American Meteorological Society*, *77*, 1275–1277.

Lindzen, R. S., Farrell, B., & Rosenthal, A. J. (1983). Absolute barotropic instability and monsoon depressions. *Journal of the Atmospheric Sciences*, *40*(5), 1178–1184. https://doi.org/10.1175/1520-0469(1983)040<1178:ABIAMD>2.0.CO;2

Madden, R. A., & Julian, P. R. (1972). Description of global-scale circulation cells in the tropics with a 40–50 day period. *Journal of the Atmospheric Sciences*, *29*(6), 1109–1123.

Moron, V., Robertson, A., & Ghil, M. (2012). Impact of the modulated annual cycle and intraseasonal oscillation on daily-to-interannual rainfall variability across monsoonal India. *Climate Dynamics*, *38*(11–12), 2409–2435. https://doi.org/10.1007/s00382-011-1253-4

Moron, V., Vautard, R., & Ghil, M. (1998). Trends, interdecadal and interannual oscillations in global sea-surface temperatures. *Climate Dynamics*, *14*(7–8), 545–569. https://doi.org/10.1007/s003820050241

Nikumbh, A. C., Chakraborty, A., Bhat, G. S., & Frierson, D. M. W. (2020). Large-scale extreme rainfall-producing synoptic systems of the indian summer monsoon. *Geophysical Research Letters*, *47*, e2020GL088403. https://doi.org/10.1029/2020GL088403

Pai, D. S., Bhate, J., Sreejith, O. P., & Hatwar, H. R. (2011). Impact of MJO on the intraseasonal variation of summer monsoon rainfall over India. *Climate Dynamics*, *36*(1), 41–55.

Plaut, G., & Vautard, R. (1994). Spells of low-frequency oscillations and weather regimes in the Northern Hemisphere. *Journal of the Atmospheric Sciences*, *51*(2), 210–236. https://doi.org/10.1175/1520-0469(1994)051

Rajeevan, M., Gadgil, S., & Bhate, J. (2010). Active and break spells of the Indian summer monsoon. *Journal of Earth System Science*, *119*(3), 229–247. https://doi.org/10.1007/s12040-010-0019-4

Sengupta, D., Goswami, B., & Senan, R. (2001). Coherent intraseasonal oscillations of ocean and atmosphere during the Asian summer monsoon. *Geophysical Research Letters*, *28*(21), 4127–4130.

Sikka, D., & Gadgil, S. (1980). On the maximum cloud zone and the ITCZ over Indian, longitudes during the southwest monsoon. *Monthly Weather Review*, *108*(11), 1840–1853. https://doi.org/10.1175/1520-0493(1980)108<1840:OTMCZA>2.0.CO;2

Singh, S., Kripalani, R., & Sikka, D. (1992). Interannual variability of the Madden–Julian oscillations in Indian summer monsoon rainfall. *Journal of Climate*, *5*(9), 973–978. https://doi.org/10.1175/1520-0442(1992)005<0973:IVOTMJ>2.0.CO;2

Thorncroft, C., & Hodges, K. (2001). African easterly wave variability and its relationship to Atlantic tropical cyclone activity. *Journal of Climate*, *14*(6), 1166–1179.

Vishnu, S., Boos, W. R., Ullrich, P. A., & O'Brien, T. A. (2020). Assessing historical variability of South Asian monsoon lows and depressions with an optimized tracking algorithm. *Journal of Geophysical Research: Atmospheres*, *977*, e2020JD032977. https://doi.org/10.1029/2020JD032977

Yasunari, T. (1979). Cloudiness fluctuations associated with the Northern Hemisphere summer monsoon. *Journal of the Meteorological Society of Japan*, *57*(3), 227–242.

Yoon, J.-H., & Chen, T.-C. (2005). Water vapor budget of the Indian monsoon depression. *Tellus*, *57*(5), 770–782. https://doi.org/10.1111/j.1600-0870.2005.00145.x

Influence of intraseasonal variability on the development of monsoon depressions

Nirupam Karmakar[1], William R. Boos[2,3], Vasubandhu Misra[1,4,5]

[1]Earth, Ocean and Atmospheric Science Department, Florida State University, Tallahassee, FL 32306, USA.

[2]Department of Earth and Planetary Science, University of California, Berkeley, USA

[3]Climate and Ecosystem Sciences Division, Lawrence Berkeley National Laboratory, Berkeley, California, USA

[4]Center for Ocean-Atmospheric Prediction Studies, Florida State University, Tallahassee, FL, USA.

[5]Florida Climate Institute, Florida State University, Tallahassee, FL, USA.

Contents of this file

Corresponding author: Nirupam Karmakar, Earth, Ocean and Atmospheric Science Department, Florida State University, Tallahassee, FL 32306, USA. (nirupam.ju@gmail.com; nkarmakar@fsu.edu)

1. Phase Composite

Phase compositing is done using a standard principal component analysis (PCA) on ISO. Similar procedure was used in *Moron et al., (1998)* to understand life cycle of low-frequency oscillatory modes in global sea surface temperature. The idea is to use the direction in the phase space which has a maximal variance. This direction is represented by the leading principal component (PC) of ISO. Let us assume $X(t)$ be the first PC obtained from ISO time series of one season (May–October) and $X'(t)$ be its time derivative (calculated using centered finite differences). Both these time series are then normalized, resulting two time series $C(t)$ and $C'(t)$, respectively, which are by construction, in approximate phase quadrature. The phase angle ($\theta(t)$) and the amplitude ($A(t)$) are calculated using the following equation:

$$\theta(t) = Arg(C'(t) + \imath C(t)) \tag{1}$$

$$A(t) = \mid C'(t) + \imath C(t) \mid \tag{2}$$

where, t denotes time, $Arg(z)$ represents the principal value of the phase of a complex number $z{=}x+iy$. $\theta(t)$ is calculated each year separately and lies between -π and π. Thus, the instantaneous state of ISO can be identified using two real scalars. The phase of ISO can be determined using $\theta(t)$, and the phase plane can be divided into eight equal intervals so that ISO at time t is said to be in phase m if

$$(m-1)\pi/4 \leq \theta(t) \leq m\pi/4, \qquad where \quad m = 1, \cdots, 8. \tag{3}$$

In addition, $A(t)$ can be used to identify 'strong' ISO episodes, which essentially determine the active and break spells. ISO is 'strong' when $A(t) \geq 1$ (Figure S1). Thus, phase composites are done using only 'strong' ISO days falling into phase m (for m=1,$\cdots$,8)

and then averaging over all the occurrences. Figure 1a in main text is constructed in this manner. Lows and depressions are considered in our analysis only when ISO exhibit 'strong' behavior. Active period of ISO is determined when positive rainfall anomaly is present over India (phases 5–7) and break period is when negative rainfall anomaly is seen over India (phases 1–3).

Reference: Moron, V., Vautard, R., & Ghil, M. (1998). Trends, interdecadal and interannual oscillations in global sea-surface temperatures. Clim. Dyn., 14 (7-8), 545–569. doi: 10.1007/s003820050241

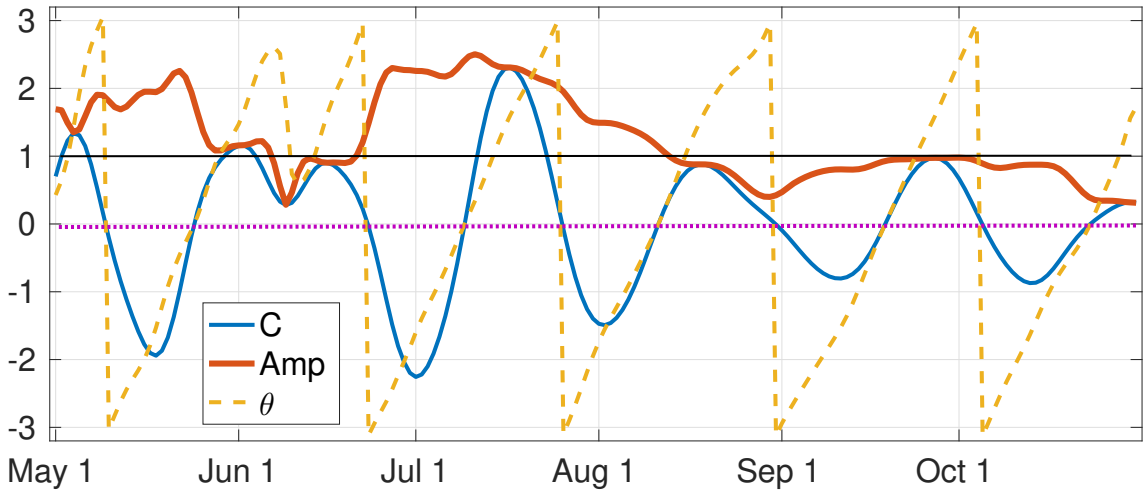

Figure S1. Example of one year (1998) to show how phase compositing is done. Normalized values of the leading PC (denoted as C), phase angle θ, and ISO amplitude (denoted as Amp) are plotted as functions of time (t). ISO is 'strong' for the days when Amp is greater than 1.

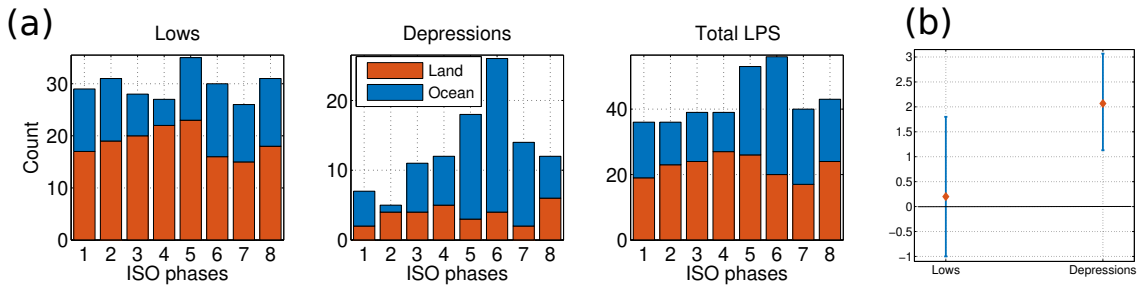

Figure S2. **(a)** Counts of 'lows', 'depressions', and 'total LPS' with genesis time in different phases of ISO (irrespective of ISO amplitude) during the same time period from Hurley-Boos dataset (1998–2012). Red and blue bars show the values for LPS formed over land and oceans, respectively. **(b)** Difference between the average number of LPS forming in active and break phases, respectively, during 1998–2012. Blue errorbars indicate 95% confidence levels in this difference calculated using 1000 bootstrap samples.

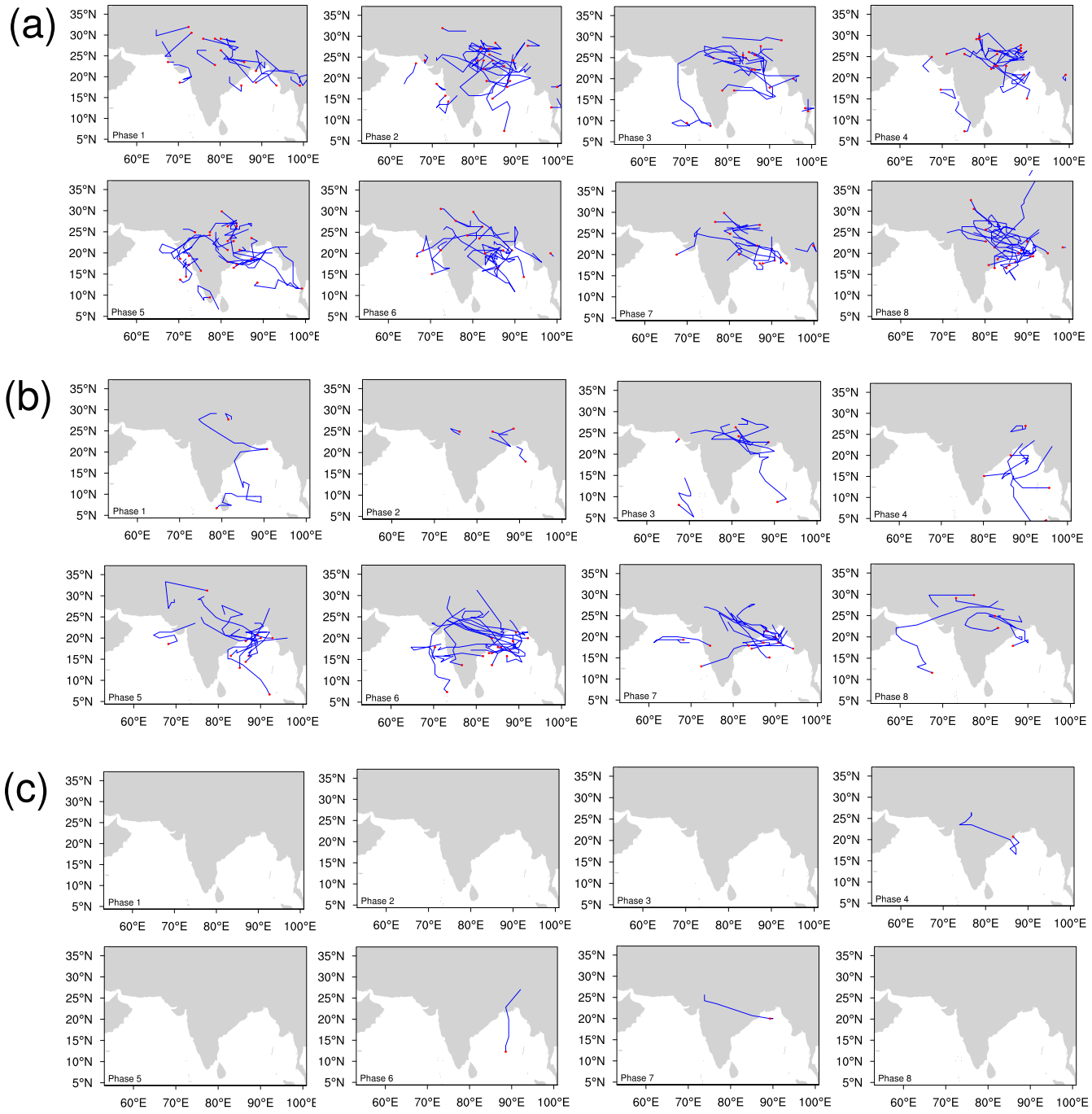

Figure S3. **(a)** Tracks of lows which developed during the eight phases of ISO as described in the main text. **(b)** Same as (a), but for depressions. **(c)** Same as (a) but for deep depressions.

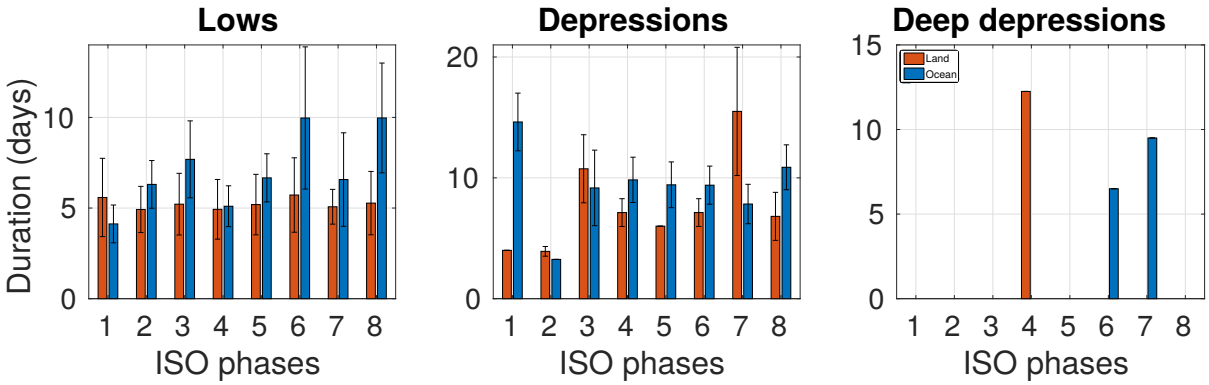

Figure S4. Duration of lows, depressions and deep depressions formed in different phases of ISO over land and oceans. Errorbars represent the spread (standard deviation) around the mean.

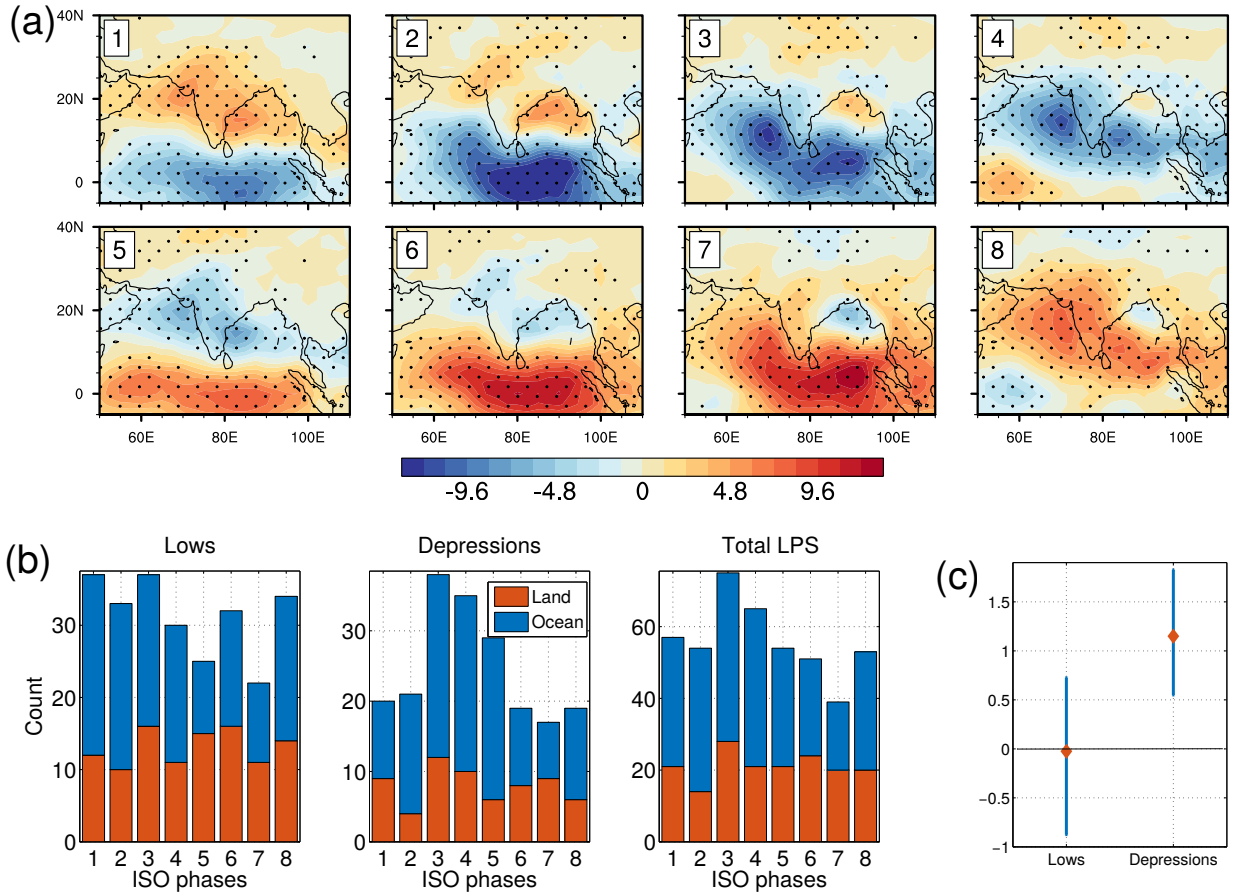

Figure S5. **(a)** Phase-composite diagram of OLR (provided by the NOAA/OAR/ESRL PSL, Boulder, Colorado, USA) ISO (in W/m^2) during May-October, 1979–2018. Only those days are considered when ISO amplitude is more than one or the ISO is 'strong'. Stippled regions are where values are significant at 5% level. Numbers in the panels indicate the phase numbers. **(b)** Counts of 'lows', 'depressions', and 'total LPS' with genesis time in different phases of ISO (when ISO is strong) during the same time period from ERA-5 track dataset (1979–2018). Red and blue bars in (b) show the values for LPS formed over land and oceans, respectively. **(c)** Difference between the average number of LPS forming in active and break phases, respectively, during 1979–2018. Blue errorbars indicate 95% confidence levels in this difference calculated using 1000 bootstrap samples. Genesis rate of lows in active and break periods are 2.30 and 2.33, respectively, per season. Genesis rate of depressions in active and break periods are 2.55 and 1.40, respectively, per season.

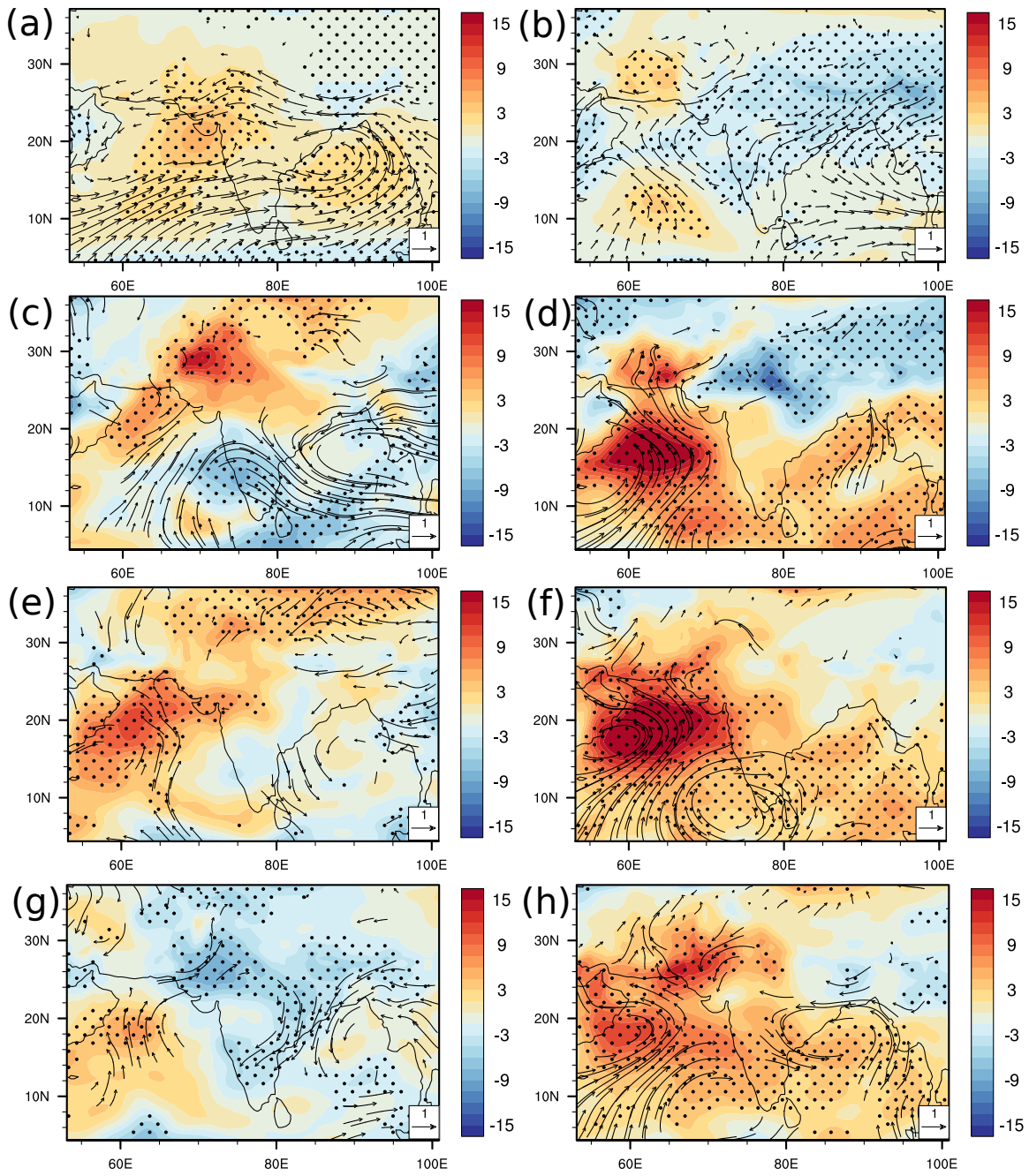

Figure S6. Vertically integrated MSE ($10^6 Jm^{-2}$) and winds (m/s) at 850 hPa anomalies during **(a)** strong active periods of ISO (602 days), **(b)** strong active periods of ISO but no LPS observed within the region (117 days), **(c)** day-(-2) for lows (10 days), **(d)** day-(-2) for depressions (10 days), **(e)** day-(-1) for lows (13 days), **(f)** day-(-1) for depressions (12 days), **(g)** day-0 for lows (21 days), **(h)** day-0 for depressions (13 days). Stippling indicate values are significant at 5% level. Only significant values of wind anomalies (at 5% level) are shown.

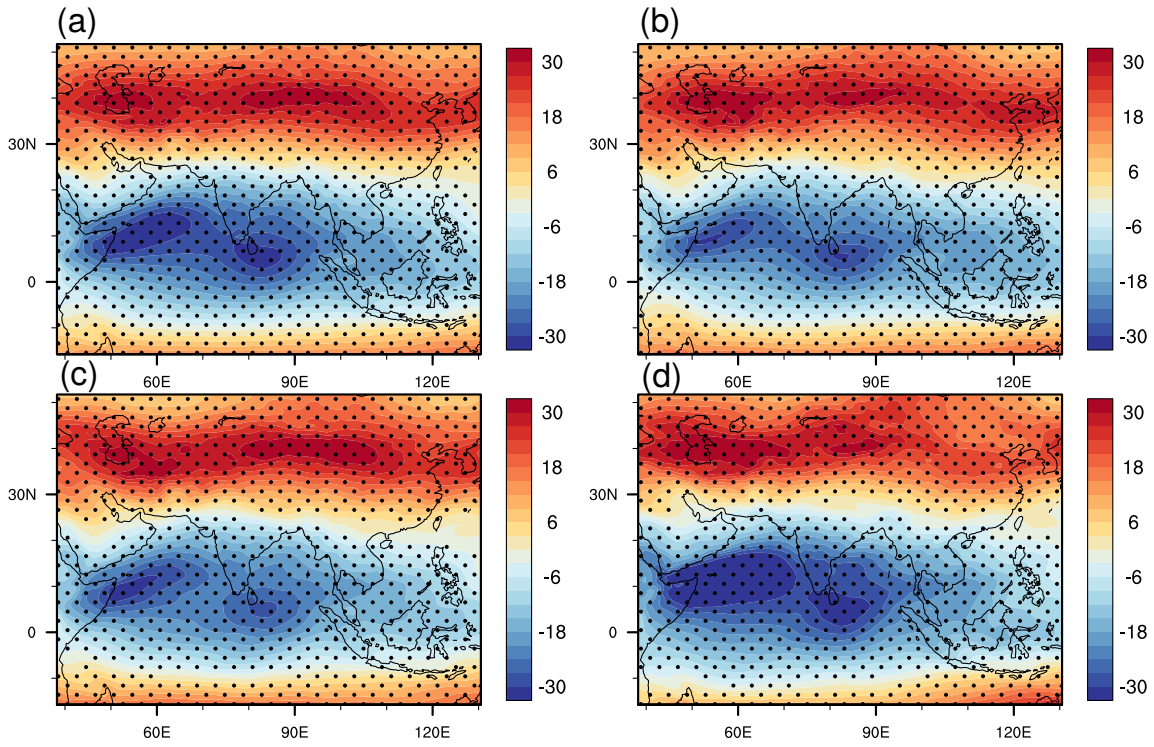

Figure S7. Vertical shear of zonal winds (m/s) during **(a)** strong active period of ISO (602 days), **(b)** strong active period of ISO but no LPS observed within the region (117 days), **(c)** genesis day for lows (21 days), **(d)** genesis day for depressions (13 days). Stippling indicate values are significant at 5% level.

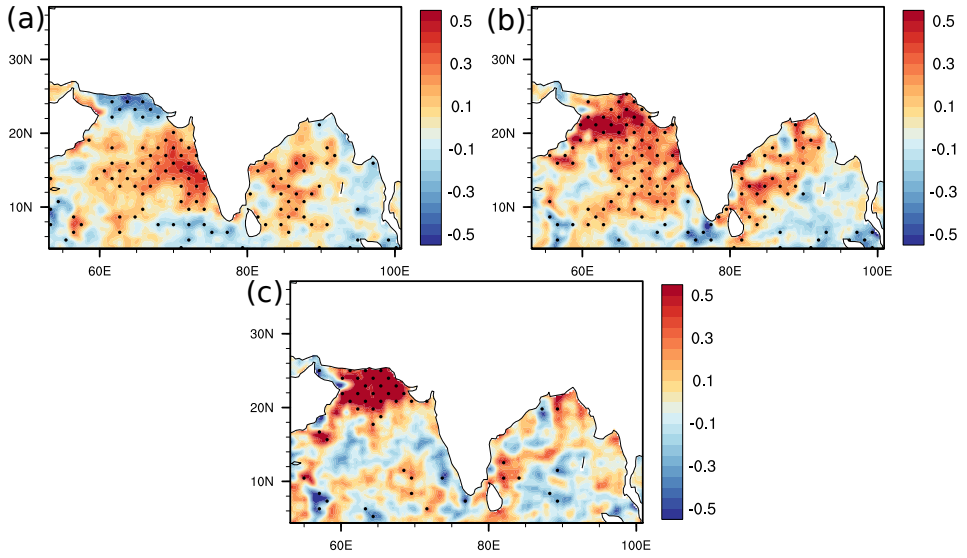

Figure S8. Sea surface temperature (K; NOAA OISST v2) anomalies during **(c)** day-0 for lows (21 days) in active periods, **(b)** day-0 for depressions (13 days) in active periods. **(c)** Difference between (b) and (a). Stippling indicate values are significant at 5% level.